Dual-Band Impedance Matching Networks Based on Split Ring Resonators for Applications in Radiofrequency Identification (RFID)

Ferran Paredes, Gerard Zamora, Jordi Bonache *Member IEEE* and Ferran Martín *Senior Member IEEE*

***Abstract*— This paper is focused on the design of dual-band impedance matching networks of interest in radiofrequency identification (RFID) systems. By cascading an impedance matching network between the chip and the antenna, the performance of the RFID tags can be improved. The main aim of this work is to demonstrate the possibility of designing such networks by means of split ring resonators coupled to microstrip transmission lines. These resonators are especially useful in this design since their equivalent circuit simplifies substantially the parameter calculation of the matching network. Dual-band conjugate matching at two different frequencies, f_1 = 867 MHz and f_2 = 915 MHz, corresponding to the assigned bands for UHF RFID in Europe and America, respectively, is demonstrated. The main difficulty for the synthesis of these dual-band matching networks relies on the proximity of f_1 and f_2. Although the chip impedance can not be considered a design parameter, the network design can be alleviated by allowing certain flexibility in the antenna stage. The fabricated prototype, a dual-band impedance matching network based on split ring resonators and loaded with a slot antenna, was characterized by measuring its reflection coefficient. The results reveal that conjugate matching at the above-cited frequencies for the chip impedance under consideration is achieved.**

***Index Terms*– Dual-band, Split Ring Resonators, Radiofrequency Identification (RFID), Impedance Matching Networks.**

I. Introduction

Artificial transmission lines have been a subject of growing interest in recent years. These structures can mimic characteristic impedance, phase shift, or other parameters of a real transmission line and therefore can be used to replace it in some specific situations. They are especially useful when some dispersive behavior not achievable with a conventional line is needed. Among these devices, it can be found the metamaterial transmission lines, that essentially are artificial structures consisting of a host propagating medium loaded with reactive elements. There are two main approaches for the synthesis of such transmission lines: (i) the CL-loaded approach, where the host line is periodically loaded with series capacitors and shunt inductors [1]-[3], and (ii) the resonant type approach, where some of the loading elements of the line are either split ring resonators [4] or complementary split ring resonators [5]. Although the same concept can be applied by using other resonators instead of split ring resonators (such as dielectric resonators, resonant stubs, etc.) these are especially useful. The reason is that the equivalent circuit model of the split ring resonator coupled to a transmission line section is quite simple. In a first order approximation it results in an LC parallel resonator cascaded with the inductance of the π model of the transmission line section, without significantly affecting the shunt capacitance of the model [4]. This is related to the fact that this resonator is excited almost exclusively by the magnetic field of the line (this can be understood through the study of the polarizability tensor of these particles [6]). This behavior can be modeled by a mutual inductance between the line and the resonator, that results, from a straightforward transformation, in the equivalent circuit previously cited.

One of the key advantages of these artificial lines is dispersion and impedance engineering. Their dispersion diagram and characteristic impedance can be engineered (to some extent) thanks to the presence of the loading elements. This is an essential characteristic that, combined with the small electrical size of such lines, makes them of actual interest for the design of high performance and compact microwave components, or devices based on novel functionalities. Although strictly speaking a minimum number of cells is needed to show some of the features of metamaterial transmission lines, it was shown in [7] that with only one cell based on the resonant approach, it is possible to control the characteristic impedance and phase shift of the resulting artificial transmission line. As it will be seen later, the strategy followed in this paper is based on this concept.

Among the wide variety of RF/microwave applications of artificial transmission lines (most of them highlighted in [8]-[10]), the design of multi-band microwave components is very promising. Dual-band operation of branch line hybrid couplers and power dividers was already demonstrated [11]-[13], and it was recently pointed out the possibility of implementing quad-band components [14]-[16]. In this work, the dual-band concept is applied to the design of impedance matching networks with extremely close operating frequencies (f_1 = 867 MHz and f_2 = 915 MHz), of interest in ultra-high-frequency (UHF) radiofrequency identification systems -RFID (UHF-RFID systems operate in the 850-

This work was supported by Spain-MEC (project contract TEC2007-68013-C02-02 METAINNOVA) and Spain MITyC through the projects FIT-330225-2007-15 and TSI-020400-2008-119, and by the Eureka Program through project 3853 METATEC. Thanks are also given to the Catalan Government (CIDEM) for funding CIMITEC and for giving support through the project 2009SGR-421. This work was also supported through the CONSOLIDER-INGENIO 2010 program (Spain-MCI) under project number CSD2008-00066.

The authors are with GEMMA/CIMITEC (Departament d'Enginyeria Electrònica), Universitat Autònoma de Barcelona. 08193 BELLATERRA (Barcelona). Spain. E-mail: ferran.martin@uab.es.

950 MHz frequency range, with multiple regulated bands around the world).

UHF-RFID is a method for identification and gathering information of objects, consisting of a reader (interrogator) and a tag (transponder). Passive tags, which are attached to the identifying objects, contain the antenna and an integrated circuit (where the information related to the object is stored), both supported by a plastic substrate (inlay). Advantages of RFID systems over bar codes are longer ranges (up to 10 m), faster speed, no need of line-of-sight, writing capability, unlimited data storage, and major robustness, among others. Disadvantages are larger size, higher cost and sensitivity to the identifying object (see [17] for further details). Size reduction and compatibility of UHF-RFID tags with the different worldwide regulated bands are challenging issues. In this paper, we pursue the second aspect. Specifically, the target is to design an impedance matching network to achieve conjugate matching between the integrated circuit and the antenna at two frequencies within the European and American bands (see f_1 and f_2 above). Although the reported example of a dual-band impedance matching network corresponds to a very specific application, the synthesis technique can be applied to many other scenarios where dual-band matching networks are required. It is particularly useful in applications where the operating frequencies are very close.

II. Requirements for the Dual-Band Impedance Matching Network

As indicated, this work is focused on the synthesis of dual-band impedance matching networks able to provide conjugate matching between the antenna and the integrated circuit in typical RFID-tags. The complete system is depicted in Fig. 1. As will be shown in the next section, the synthesis technique of the dual-band impedance matching network is based on a perturbation method, which is useful in those situations where the required characteristics of the network at the two operating frequencies do not differ too much (as is the case of conjugate matching in typical RFID-tags).

Conjugate matching between the antenna and the integrated circuit at a single frequency can be achieved by means of a transmission line with a certain value of the characteristic impedance and electrical length (or phase constant) at that frequency. Such line characteristics are determined simply by forcing the impedance of the antenna to be the conjugate of the impedance seen from the input port of the transmission line (considering that it is loaded with the integrated circuit at the output port). However, for dual-band operation, there is no solution with a conventional line. More complex networks can be used, or, alternatively, we can implement the dual-band impedance matching network by means of an artificial transmission line, with more degrees of freedom. The target is to obtain the necessary characteristic impedance and phase constant at the two operating frequencies in order to achieve conjugate matching.

Let us now consider a typical integrated circuit for the RFID-tag. The impedance of this integrated circuit at the intended operating frequencies, f_1 and f_2, is $Z_{IC}(f_1)=22-j404\ \Omega$ and $Z_{IC}(f_2)=16-j380\ \Omega$, respectively. With regard to the antenna, there are many different configurations. In this work, we have considered a slot antenna for simplicity. The main aim of this work is the proposal of a synthesis method for the implementation of dual-band impedance matching networks, rather than fabricating a functional RFID-tag. Thus, we will implement the antenna and the impedance matching network on a commercial low loss microwave substrate, the *Rogers RO3010* substrate with dielectric constant $\varepsilon_r=10.2$ and thickness $h=1.27$ mm (available in our laboratory). The impedance of this antenna (Fig. 2) at the design frequencies is $Z_a(f_1)=1.65-j67.7\ \Omega$ and $Z_a(f_2)=1.13-j59.6\ \Omega$. Notice that the frequency dependence of the impedance around the resonance does neither correspond to a series nor to a parallel RLC circuit, since neither the imaginary part of the impedance vanishes at the frequency where the real part achieves its maximum value (parallel RLC circuit) nor the real part remains constant around the frequency range where the imaginary part vanishes (series RLC circuit). This is due to the presence of distributed effects in the antenna structure. However, by varying the position of the port reference, the structure behaves as a parallel RLC circuit, and this allows for instance to compute the radiation resistance or conductance.

From the impedance values of the integrated circuit and the antenna at the system frequencies, the requirements for the artificial transmission line (impedance matching network) are: characteristic impedance $Z_{B1}=91.18\ \Omega$ and electrical length $\phi_1=\beta l=113.9^o$ at f_1, and $Z_{B2}=84.67\ \Omega$ and $\phi_2=\beta l=112.6^o$ at f_2.

III. Design of the Dual-Band Impedance Matching Network Based on Split Ring Resonators: Modeling and Analysis

Let us now consider, in view of the above requirements on phase and characteristic impedance at the two operating frequencies, how to implement the impedance matching network. This network must provide a positive phase shift at both frequencies, with a smaller phase at the upper frequency, and simultaneously satisfy the characteristic impedance requirements ($Z_B=91.18\ \Omega$ at f_1 and $Z_B=84.67\ \Omega$ at f_2). This can be achieved by means of an artificial line consisting of a microstrip line loaded with a split ring resonator, as shown in Fig. 3. The geometry of the split ring resonator and its distance to the line, the characteristic impedance and length of the host line, and the relative position of the split ring resonator along the line, are the potential control parameters (we need at least four independent parameters since we have four conditions). This configuration is similar to some filter designs based on reactively coupled resonators [18], but in this case our objective is to adjust the phase and characteristic impedances to some specific values rather than the transmission characteristics of the structure.

Let us now demonstrate that the proposed configuration (Fig. 3) is adequate in order to satisfy the required phase and characteristic impedance for the impedance matching network at the two operating frequencies. We can do that by considering that the structure is composed of two transmission line sections sandwiching a split ring resonator loaded line in a cascade configuration. As long as the split ring resonator is electrically small, the central network can be modeled by means of a lumped element model [19]. In this

model, depicted in Fig. 4 for completeness, C'_s and L'_s are related to the inductance, L_s, and capacitance, C_s, of the split ring resonator according to

$$L'_s = 2M^2 C_s \omega_o^2 \tag{1}$$

$$C'_s = \frac{L_s}{2M^2 \omega_o^2} \tag{2}$$

where M is the mutual coupling between the host line and the split ring resonator and $\omega_o=(L_sC_s)^{-1/2}=(L'_sC'_s)^{-1/2}$ is the resonance frequency of the resonator. As reported in [19], the series inductance of the lumped element model of Fig. 4 is given by

$$L' = L - L'_s \tag{3}$$

where L denotes the inductance of the host line segment where the split ring resonator is coupled. Under conditions of weak coupling (which will be justified in the next section), L'_s is small (see expression 1) and $L' \approx L$. Thus, L' and C can be considered to be the line parameters of the transmission line section corresponding to the region occupied by the split ring resonator. To simplify the model, we can now consider either half of this transmission line section as an extension of the adjacent lines, and model the whole structure as shown in Fig. 5. In this figure, Z_o and k are the characteristic impedance and phase constant, respectively, of the host line, l is the whole length of the network and l' is the distance between the position of the split ring resonator in the line and the left hand side extreme of the line.

The dispersion relation of the structure of Fig. 5 (in the regions where propagation is allowed) can be inferred from its transmission matrix according to [9,18]

$$\cos \beta l = \frac{A+D}{2} \tag{4}$$

where β is the phase constant, and A and D are the diagonal elements of the transmission matrix. Such matrix can be inferred from the product of the transmission matrices of the three two-ports forming the structure. After some simple algebra, the following result is obtained:

$$\cos \beta l = \cos kl - \frac{\chi}{2Z_o} \sin kl \tag{5}$$

where χ is the reactance of the tank formed by C'_s and L'_s. Notice that the dispersion diagram does not depend on the relative position of the split ring resonator in the line (i.e., the phase constant β depends on l, but not on l'). However, the characteristic impedance (or image impedance for a single unit cell structure) given by

$$Z_B = \frac{2B}{D - A + 2\sqrt{\left(\frac{A+D}{2}\right)^2 - 1}} \tag{6}$$

for non-symmetrical networks [9,18], does depend on l', since B and D-A depend on it. For the network of Fig. 5:

$$B = j(Z_o \sin kl + \chi \cos k(l-l') \cos kl') \tag{7}$$

$$D - A = \chi Y_o \sin k(l - 2l') \tag{8}$$

and the characteristic impedance can be inferred by introducing (5), (7) and (8) in (6). Since B is purely imaginary, D-A is real, and the square root in (6) is purely imaginary, the characteristic impedance in the transmission band is actually a complex number for non-symmetrical networks. Notice that for symmetric networks D–A=0, and Z_B is real. Although the required characteristic impedance of the dual-band impedance matching network is real, we will consider in principle a non-symmetrical network because, as will be latter shown, the imaginary part of Z_B is small (hence, it can be neglected) and l' can be used as a control parameter in order to adjust the real part of the impedance to the required values at the design frequencies.

The technique for the synthesis of the impedance matching network is based on a perturbation method. This is reasonable since, due to the proximity of the operating frequencies, the target characteristic impedances and electrical lengths of the artificial transmission line at these frequencies are similar. Specifically, we will consider the structure as composed of a host line perturbed by the presence of the split ring resonator. Hence, the required line parameters at the operating frequencies can be considered to result as consequence of the perturbation produced by the split ring resonator around the central values corresponding to the unperturbed line. According to this, the host line must be designed to provide an unperturbed (i.e., with χ=0) electrical length and characteristic impedance at the central frequency ($f_c=(f_1+f_2)/2$) of $\phi(f_c,\chi=0)=(\phi_1+\phi_2)/2$ and $Z_o=(Z_{B1}+Z_{B2})/2$, respectively (obviously, the characteristic impedance of the unperturbed line does not depend on frequency). From these values, the geometry (length and width) of the host transmission line is perfectly determined. To this end, we introduced our substrate parameters (see section II) into the *Line Calc* transmission line calculator (integrated in *Agilent ADS*).

Let us now focus on the determination of the characteristics of the parallel resonant tank and its position in the line. Since the required electrical length at the operating frequencies varies smoothly as compared to the value at the central frequency of the unperturbed structure, we can express the electrical length as a perturbation around the central value by using a first order Taylor expansion as follows:

$$\phi(f,\chi) = \phi(f_c,0) + \left.\frac{\partial \phi(f,\chi)}{\partial f}\right|_{f_c,\chi=0} (f - f_c) + \left.\frac{\partial \phi(f,\chi)}{\partial \chi}\right|_{f_c,\chi=0} \chi \tag{9}$$

In the previous expression, the electrical length is only a function of f and χ since the length of the line was already fixed. From expression (9), we can determine the value of χ at f_2 (χ_{f2}) by forcing the electrical length to be ϕ_2 at this frequency. Obviously, due to linearization, $\chi_{f1}= -\chi_{f2}$. Thus, we obtain two conditions for the determination of the inductance and capacitance of the parallel resonant tank of the model of Fig. 5.

Similarly, the characteristic impedance of the network can be linearized in the variables f and χ as follows:

$$Z_B(f,\chi,l') = Z_B(f_c,0,l') + \left.\frac{\partial Z_B(f,\chi,l')}{\partial f}\right|_{f_c,\chi=0} (f - f_c) + \left.\frac{\partial Z_B(f,\chi,l')}{\partial \chi}\right|_{f_c,\chi=0} \chi \tag{10}$$

Notice that this impedance not only depends on f and χ, but also on l'. Actually, in the right-hand side member of (10),

neither the first term nor the second one are dependent of l'. The reason is that $Z_B=Z_o$ for $\chi=0$, and the dependence in the partial derivative of Z_B with frequency vanishes for $f=f_c$ and $\chi=0$. Thus, only the third term depends on the position of the split ring resonator in the line. This simplifies the determination of l'. To this end, we neglected the imaginary part in (10), and we swept l' until the characteristic impedances Z_{B1} and Z_{B2} at the design frequencies were obtained. Due to linearization, the value of l' necessary to obtain Z_{B1} at f_1 also provides Z_{B2} at f_2.

IV. RESULTS AND DISCUSSION

The calculation of the electrical length (9) and the characteristic impedance (10) is obtained, respectively:

$$\phi(f,\chi)=\phi(f_c,0)+\frac{2\pi l}{v_p}(f-f_c)+\frac{1}{2Z_o}\chi \qquad (11)$$

$$Z_B(f,\chi,l')=Z_B(f_c,0,l')+$$
$$+\frac{1}{2\sin kl}\left(2\cos k(l-l')\cos kl'+j\sin k(l-2l')\right)\chi \qquad (12)$$

where v_p in (11) denotes the phase velocity of the unperturbed line. From (11) and (12), $\chi_{f1}(=-\chi_{f2})$ and l' can be isolated (as indicated in the previous section). The values are $\chi_{f1}=-\chi_{f2}=11.35\ \Omega$ and $l'=2.6$ cm. From the values of the reactance at the design frequencies, the inductance and capacitance of the resonant tank are found to be $L'_s=109.3$ pH and $C'_s=292$ pF, respectively. Finally, the length and width of the host line, determined with the help of *Agilent ADS* as indicated above, are found to be $l=4.2$ cm and $W=0.275$ mm, respectively.

We simulated the structure of Fig. 5 considering the parameters given in the previous paragraph with the help of *Agilent ADS*. From the resulting S-parameters, we inferred the parameters of the transmission matrix, and from them, we obtained the dispersion relation as well as the dependence of the characteristic impedance with frequency. The results are depicted in Fig. 6. As expected, the required electrical length and characteristic impedance (real part) are obtained at the design frequencies. The imaginary part of the characteristic impedance is small as compared to the real part. This justifies the consideration of the non-symmetric structure to achieve the target network requirements. The consideration of a symmetric structure with the split ring resonator in the central position of the line would be another possibility, but in this case the synthesis technique is not so simple because a degree of freedom is lost (the position of the split ring resonator l' is fixed), since we cannot set the impedance of the host line to $Z_o=(Z_{B1}+Z_{B2})/2$. Rather than this, the antenna impedance Z_a should be in this case the fitting parameter (instead of l'), but this complicates the synthesis of the network.

With regard to the split ring resonators, we chose a combination of internal radius (r_{in}) which represents the distance from the center to inner edge of the inner ring as depicted in figure 3(a); external radius (r_{ext}) from the center to inner edge of the outer ring; rings width (c) and inter-rings distance (d) that provided the required resonance frequency, namely, $f_o=(L'_sC'_s)^{-1/2}/2\pi$. The model reported in [20] was considered but, as usual, we optimized the geometry of the split ring resonators (L_s and C_s) in order to adjust the resonance frequency to the target value. By varying the distance between the host line and the split ring resonator, l_{SRR}, the mutual coupling M can be tailored and adjusted to obtain the required value of L'_s and C'_s. In practice, we determined l_{SRR} by adjusting the characteristic impedance (real part) and electrical length to the target values at the operating frequencies. This was done by using the *Agilent Momentum* commercial software. Following this procedure, we finally obtained the following geometrical parameters: internal radius $r_{in}=7.2$ mm, external radius $r_{ext}=8.4$ mm, rings width $c=0.5$ mm, inter-rings distance $d=0.2$ mm and distance between host line and SRR $l_{SRR}=0.5$ mm (which results in weak coupling). Although the gap dimensions of the rings are not a design parameter, in this design we used a $gap=0.4$ mm. The complete layout of the dual-band impedance matching network is that depicted in Fig. 3, and the resulting dispersion diagram and characteristic impedance (inferred from the electromagnetic simulation of the network) are also depicted in Fig. 6 for comparison purposes. The figure shows that the target values of phase and impedance are achieved at the desired frequencies and also the small contribution of the imaginary part of Z_B, validating the simplification of expression (12).

The whole layout is depicted in Fig. 7(a), where the RFID chip is modeled with a port with frequency dependent impedance. The structure is composed of the designed dual-band matching network between the slot antenna and the chip. This structure was simulated through the *Agilent Momentum* commercial software and the prototype was measured by means of the *Agilent E8364B* vector network analyzer. Since the impedance of the measuring probes was 50 Ω (i.e., do not corresponding to the chip impedance), a renormalization of the port impedance was necessary. This procedure was carried out by means of a de-embedding process and re-simulation with the chip impedance by means of the commercial software *Agilent ADS*. Specifically, we obtained the measured return loss, S_{11}, seen from the input of the impedance matching network (see Fig. 7a), obviously with a 50 Ω reference impedance. These results were then exported to the *Agilent ADS*, from which it was possible to infer the power wave reflection coefficient, s, [21,22] by considering the impedance of the integrated circuit as reference impedance of the input port. Fig 7(b) illustrates the simulated (electromagnetic simulation with losses and circuit simulation –circuit of Fig. 5– without losses) and measured (through the explained procedure) reflection coefficient for the fabricated structure. By comparing all the responses, good agreement can be observed, although the measurement and electromagnetic simulation by including losses present certain degradation due to the effect of losses. The values of the reflection coefficient extracted from measurement at the target frequencies are in the vicinity of 10 dB. These values correspond to an input impedance of $Z_{in}(f_1)=38+j397\ \Omega$ and $Z_{in}(f_2)=33+j400\ \Omega$ at desired frequencies. These values are enough to obtain the typical required reading ranges for RFID applications [23]. To evaluate the level of losses introduced by the structure we carried out a full wave simulation of the

propagation through the matching network normalized to the real part of the target impedance of such network (91.18 Ω at 867 MHz and 84.67 Ω at 915 MHz). For this purpose we considered a linear variation of the port impedance with frequency. In Fig. 8(a), it can be seen that the losses introduced by the network are not significant in the frequencies of interest (0.2 dB). We also obtained the $|S_{11}|^2+|S_{21}|^2$ response (Fig 8(b)), where it can be seen that the power loss is only a small fraction of the incident power (5%) at the frequencies of interest.

These results can be compared with the minimum reflection coefficient achievable with an optimal lossless broadband matching network, determined by the Bode's limit [24,25]. The input impedance of the chip is mainly determined by the voltage multiplier stage of the integrated circuit transponder, which can be modeled by a parallel combination of a resistance R_C (that accounts for the losses of the multiplier) and a capacitance C_C (that includes all the capacitive effects) [26,27]. According to Bode's limit, the reflection coefficient achievable by any passive and lossless network placed between a purely resistive generator (in our case the antenna) and a *RC* parallel load is limited by the expression

$$\int_0^\infty \ln\left(\frac{1}{|\rho|}\right) d\omega \le \frac{\pi}{R_C C_C} \tag{13}$$

where ρ denotes the reflection coefficient, ω the angular frequency and R_C and C_C are the equivalent resistance and capacitance of the chip, respectively. If a good impedance matching within some frequency range is desired, the best results can be obtained if $|\rho|=1$ at all frequencies except in the band of interest [28]. Under this assumption, and considering a constant value of $|\rho|$ across the band of interest (where impedance matching is pursued), expression (13) becomes:

$$2\ln\left(\frac{1}{|\rho|_{\max}}\right)(f_2 - f_1) \le \frac{1}{R_C C_C} \tag{14}$$

The values of R_C and C_C can be obtained from the input impedance of the chip transformed to its equivalent *RC* parallel circuit. The evaluation of (14) shows that the Bode's limit for the chip considered in this work is 25 dB all over the band from f_1 to f_2, assuming an infinite number of elements for the matching network (square shaped response). Moreover, in such analysis, the antenna was modeled as a resistor, which represents an unlimited bandwidth for the antenna. Nevertheless, from the simulated results, it can be seen that for the structure of figure 7 the matching level is 28 dB (in the lossless case) at the two desired frequencies. Furthermore, in such case, the antenna was not modeled as a resistor, although its impedance exhibits a very small variation in the band of interest. Even so, the dimensions of the planar antennas used in this type of applications are a critical point, and it is well known that this reduction in the antenna size implies a drastically reduction of its bandwidth according to Chu's theorem concerning to physical limitations of any antenna [29,30]. Due to this reason, a substantial reduction of the limit given by (14) is expected in practical RFID tags. Thus, in summary, the dual-band matching networks based on SRRs presented in this work are very convenient in order to achieve the required matching at the desired RFID frequency bands with a small number of elements.

V. Conclusion

In conclusion, the potential use of split ring resonators coupled to microstrip transmission lines to the design of radiofrequency identification (RFID) tags with dual-band capability is demonstrated. Specifically, a design procedure for dual-band matching networks based on a perturbation method was presented. The matching structure, was designed to provide conjugate matching between the antenna and the RFID chip at two different frequencies. Such frequencies were chosen to be the UHF RFID bands in Europe and America (f_1=867 MHz and f_2=915 MHz, respectively). The novel ideas introduced in this paper were validated through the fabrication of a prototype device, consisting of the dual-band impedance matching network and a slot antenna. The simulated and measured results corroborate that conjugate matching at the target frequencies is achieved, with a good level of return losses. The perturbation method reported is of special interest for the design of dual-band impedance matching networks in applications where the operating frequencies are extremely close.

References

[1] A. K. Iyer and G. V. Eleftheriades. "Negative refractive index metamaterials supporting 2-D waves," in *IEEE-MTT Int'l Microwave Symp.*, vol. 2, Seattle, WA, pp. 412– 415, June 2002.

[2] A. A. Oliner. "A periodic-structure negative-refractive-index medium without resonant elements," in *URSI Digest, IEEE-AP-S USNC/URSI National Radio Science Meeting,* San Antonio, TX, pp. 41, June 2002.

[3] C. Caloz and T. Itoh. "Application of the transmission line theory of left-handed (LH) materials to the realization of a microstrip LH transmission line," *in Proc.IEEE-AP-S USNC/URSI National Radio Science Meeting,* vol. 2, San Antonio, TX, pp. 412–415, June 2002.

[4] F. Martín, F. Falcone, J. Bonache, R. Marqués and M. Sorolla, "Split ring resonator based left handed coplanar waveguide", *Appl. Phys. Lett.*, vol. 83, pp. 4652-4654, December 2003.

[5] F. Falcone, T. Lopetegi, M.A.G. Laso, J.D. Baena, J. Bonache, R. Marqués, F. Martín, M. Sorolla, "Babinet principle applied to the design of metasurfaces and metamaterials", *Phys. Rev. Lett.*, vol. 93, p 197401, November 2004.

[6] J. García-García, F. Martín, J.D. Baena, R.Maques, "On the resonances and polarizabilities of split ring resonators", *J. Applied Physics*, vol. 98, pp. 033103-1-9, September 2005.

[7] M. Gil, I. Gil, J. Bonache, J. García-García and F. Martín, "Metamaterial transmission lines with extreme impedance values", *Microwave and Optical Technology Letters*, vol. 48, pp. 2499-2505, December 2006.

[8] G.V. Eleftheriades and K.G. Balmain Editors, *Negative Refraction Metamaterials: Fundamental Principles and Applications*, John Wiley & Sons, Inc, New York, 2005.

[9] C. Caloz and T. Itoh, *Electromagnetic Metamaterials: Transmission Line Theory and Microwave Applications*, John Wiley & Sons, Inc. New York, 2006.

[10] R. Marqués, F. Martín and M. Sorolla, *Metamaterials with Negative Parameters: Theory, Design and Microwave Applications*, John Wiley & Sons, Inc, New York, 2007.

[11] I.H. Lin, M. De Vincentis, C. Caloz and T. Itoh, "Arbitrary dual-band components using composite right/left handed transmission lines", *IEEE Trans. Microwave Theory and Techniques*, vol. 52, pp. 1142-1149, April 2004.

[12] J. Bonache, G. Sisó, M. Gil, A. Iniesta, J. García-Rincón and F. Martín, "Application of composite right/left handed (CRLH) transmission lines based on complementary split ring resonators (CSRRs) to the design of

dual-band microwave components", *IEEE Microwave Wireless Comp. Lett.*, vol. 18, pp. 524-526, August 2008.
[13] G. Sisó, J. Bonache and F. Martín, "Dual-band Y-junction power dividers implemented through artificial lines based on complementary resonators", *IEEE-MTT-S Int'l Microw. Symp. Digest,* pp. 663-666, Atlanta, Georgia, June 2008.
[14] A. Rennings, S. Otto, J. Mosig, C. Caloz, and I. Wolff, "Extended composite right/left-handed (E-CRLH) metamaterial and its application as quadband quarter-wavelength transmission line," in *Proc. Asia-Pacific Microwave Conference (APMC)*, Yokohama, Japan, Dec. 2006.
[15] G.V. Eleftheriades, "A generalized negative-refractive-index transmission-line (NRL-TL) metamaterial for dual-band and quad-band applications", *IEEE Microwave Wireless Comp. Lett.*, vol. 17, pp. 415-417, June 2007.
[16] G. Sisó, M. Gil, J. Bonache and Martín, "Generalized Model for Multi-Band Metamaterial Transmission Lines", *IEEE Microwave Wireless Comp. Lett.*, vol. 18, pp. 728-730, November 2008.
[17] V. D. Hunt, A. Puglia, M. Puglia, *RFID: A Guide to Radio Frequency Identification*, John Wiley & Sons, Inc. New York, 2007.
[18] D.M. Pozar, *Microwave Engineering*, Addison Wesley, 1990.
[19] F. Aznar, J. Bonache and F. Martín, "An improved circuit model for left handed lines loaded with split ring resonators", *Appl. Phys. Lett.*, vol. 92, paper 043512, February 2008.
[20] J.D. Baena, J. Bonache, F. Martín, R. Marqués, F. Falcone, T. Lopetegi, M.A.G. Laso, J. García, I Gil, M. Flores-Portillo and M. Sorolla, "Equivalent circuit models for split ring resonators and complementary split rings resonators coupled to planar transmission lines", *IEEE Trans. Microwave Theory Tech.*, vol. 52, pp. 1451-1461, April 2005.
[21] K.Kurokawa, "Power waves and the scattering matrix", *IEEE Trans. Microw. Theory Tech.*, vol. MTT-13, no. 3, pp. 194–202, Mar. 1965.
[22] P.V. Nikitin, K.V. Seshagiri Rao, S.F. Lam, V. Pillai, R. Martinez, and H. Heinrich, "Power Reflection Coefficient Analysis for Complex Impedances in RFID Tag Design", *IEEE Trans. Antennas and Propagation,* vol. 53, pp. 2721-2725, September 2005.
[23] K. V. Seshagiri Rao, P.V. Nikitin, and S.F. Lam, "Antenna design for UHF RFID tags: a review and a practical application", *IEEE Trans. Antennas and Propagation,* vol. 53, pp. 3870-3876, December 2005.
[24] H. W. Bode, "Network analysis and feedback amplifier design", pp. 360-371. D. Van Nostrand co. New York, N.Y., 1945.
[25] R. M. Fano, "'Theoretical Limitations on the Broadband Matching of Arbitrary Impedances," Journal of the Frank1in Institute, Vol. 249, pp. 57-84 and 139-154 (January -February 1950).
[26] E. Bergeret, J. Gaubert, P. Pannier and J.M. Gaultier, "Modeling an design of CMOS UHF voltage multiplier for RFID in a EEPROM compatible process" *IEEE Trans. Circuits and Systems,* vol. 54, pp.833-837, October 2007.
[27] G. De Vita and G. Iannaccome, "Design Criteria for the RF section of UHF and microwave passive RFID transponders", *IEEE Trans. Microwave Theory Tech.*, vol. 53, no. 9, pp. 2978-2990, September 2005.
[28] G. L. Matthaei, L. Young, and E. M. T. Jones, *Microwave filters, impedance-matching networks and coupling structures*, Artech House Books, Dedham, Mass. 1980.
[29] H. A. Wheeler, "Fundamental Limitations of Small Antennas" *Proc. IRE*, vol. 35, pp 1479-1484, December 1947.
[30] L. J. Chu, "Physical limitations in omnidirectional antennas", *J Appl. Phys*, vol. 19, pp. 1163–1175, 1948

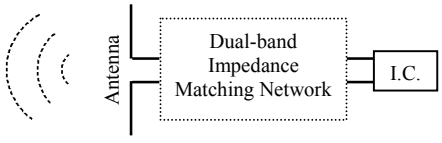

Fig. 1. Schematic of a dual-band RFID-tag including the antenna, the integrated circuit and the dual-band impedance matching network.

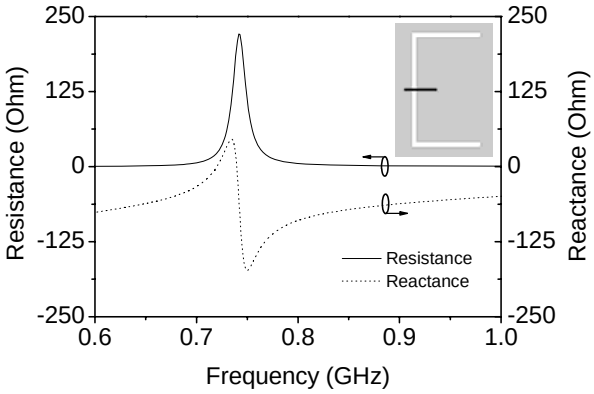

Fig. 2. Impedance of the considered slot antenna. Dimensions are given in Fig. 7. Notice that the resonance frequency of the antenna (0.75GHz) is different than the resonances of the system (composed of the antenna, the dual-band impedance matching network and the chip), namely, f_1 and f_2 (see Fig. 7).

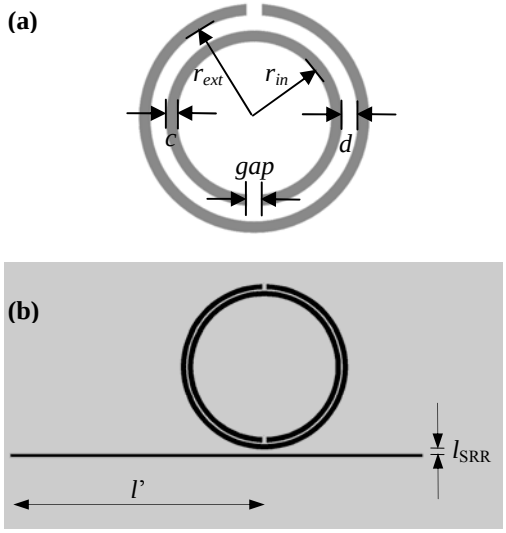

Fig. 3. (a) Topology of the *SRR* (in this figure, grey zones represent the metallization). (b) Proposed dual-band impedance matching network based on a microstrip line loaded with a split ring resonator; *l'* is the distance between the position of the split ring resonator in the line and the left hand side extreme of the line. The subscript *SRR* stands for split ring resonator.

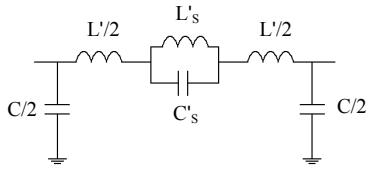

Fig. 4. Lumped element equivalent circuit model of a microstrip line section loaded with a split ring resonator.

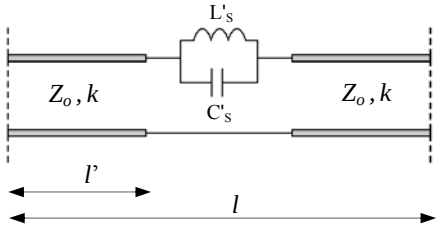

Fig. 5. Model of the dual-band impedance matching network of Fig. 3.

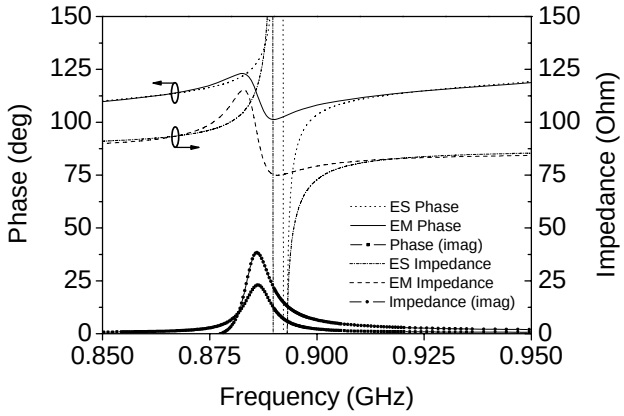

Fig. 6. Dependence of the characteristic impedance with frequency and phase response for the designed dual-band impedance matching network (electromagnetic and electric simulation); the small values of imaginary part of phase and impedance at the design frequencies can be neglected.

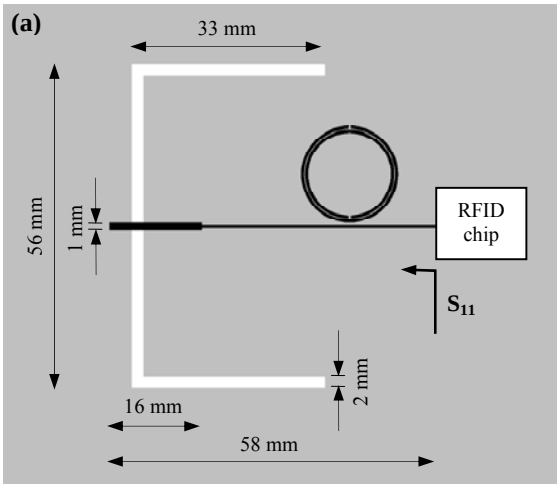

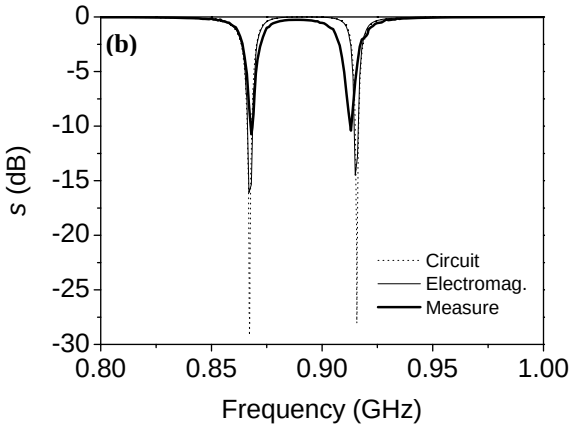

Fig. 7. (a) Topology of the designed system consisting of the dual-band matching network between the slot antenna and RFID chip. The metallic parts are depicted in black on the top layer and in gray in the bottom layer. The slot antenna is etched on the bottom layer and depicted in white. (b) Electromagnetic simulation (by including losses), circuit simulation (without losses) and measured return loss of the fabricated device.

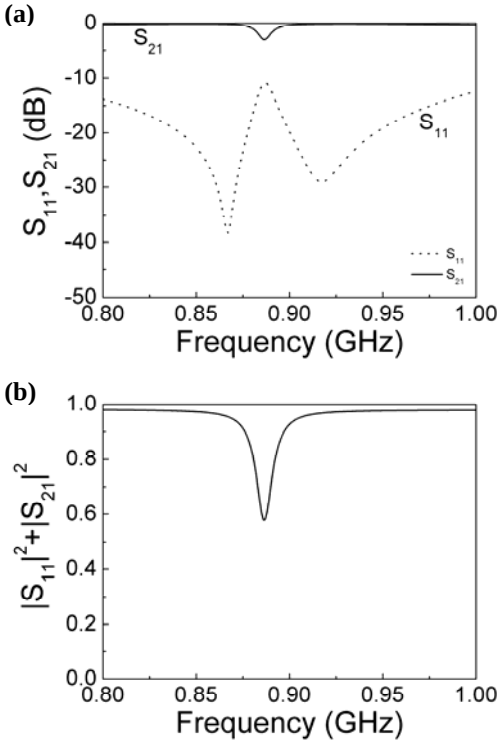

Fig 8. (a) Full wave simulation of the *S* parameters and (b) $|S_{11}|^2+|S_{21}|^2$ relation for the structure of Fig. 3.